




# Anisotropic behavior and mechanical properties of Ti-6Al-4V alloy in high temperature deformation

Song Gao<sup>1,\*</sup> , Tonggui He<sup>1</sup>, Qihan Li<sup>1</sup>, Yingli Sun<sup>1</sup>, Ye Sang<sup>1</sup>, Yuhang Wu<sup>1</sup>, and Liang Ying<sup>2</sup>

<sup>1</sup>School of Mechatronic Engineering, Changchun University of Technology, Changchun 130012, Jilin, China

<sup>2</sup>School of Automotive Engineering, Dalian University of Technology, Dalian 116024, China

Received: 1 June 2021

Accepted: 13 September 2021

Published online:  
3 January 2022

© The Author(s), under exclusive licence to Springer Science+Business Media, LLC, part of Springer Nature 2021

## ABSTRACT

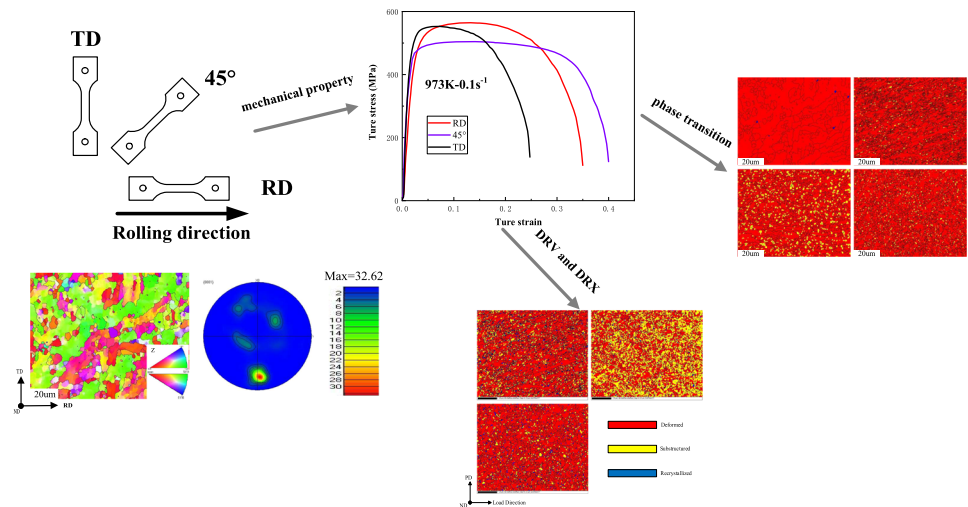
Uniaxial hot tensile tests were carried out in the RD, 45°, and TD directions of cold-rolled Ti-6Al-4V alloy sheets. At 973 K-0.1 s<sup>-1</sup>, it shows apparent mechanical and fracture anisotropy. Increasing temperature or decreasing strain rate can reduce the anisotropic behavior and significantly improve its forming quality. The SEM-EBSD result indicates that there is a T-type texture in the initial microstructure. The yield anisotropy is closely related to the distribution of the Schmid factor caused by the texture. In the RD and 45° loading paths, the Schmid factors are large, and the basal and prismatic slip is easy to be activated. It is difficult to activate these two slip systems in the TD loading direction. Under high-temperature loading conditions, the rotation of grains leads to different orientation dispersion, which further affects the phase transformation and softening behavior. The primary mechanism affecting the softening behavior is dynamic recovery (DRV). In the case of the 45° loading direction, the orientation dispersion is the largest. Its DRV and phase transformation behavior is more prominent than the other two loading directions. The loading along 45° direction has the best forming quality, and it can be selected in the processing of Ti-6Al-4V alloy.

Handling Editor: Naiqin Zhao.

Address correspondence to E-mail: gaosong@ccut.edu.cn

<https://doi.org/10.1007/s10853-021-06569-8>

## GRAPHICAL ABSTRACT



## Introduction

The high-performance Ti-6Al-4V alloy is an advanced structural material widely used in the aerospace industry due to its excellent corrosion resistance, low density, and high specific strength [1–3]. The precise forming of such high-performance, lightweight materials has always been a hot issue and the frontier in the metal material processing field. Since the titanium alloy has a close-packed hexagonal structure at room temperature, it has the characteristics of few slip systems, considerable deformation resistance, poor plasticity, and a narrow processing window. Generally, the hot forming technology is always used to process this kind of hard-to-deform material [4–6]. Under the effect of the thermodynamic field, the deformation mechanism and flow characteristics of the Ti-6Al-4V are sensitive to temperature and strain rate [7–9]. Besides, due to anisotropy, it shows different yield strengths and ductility in the different loading directions. This characteristic will significantly affect the formability and the service performance of the formed parts. Therefore, it is crucial to study the flow characteristics and anisotropic behavior in the hot forming process.

In recent years, many scholars have carried out much experimental research on the mechanical

properties of Ti-6Al-4V alloy from macro and micro perspectives. In early research, temperature and strain rate effects on mechanical properties are well studied [10–14]. To determine the deformation mechanism, most of these researches have carried out microstructure observation through SEM. Many constitutive models are established to describe mechanical behavior [10–12]. With the development of research, the effect of initial microstructure on its mechanical properties has been extensively studied. Salishchev and Zherebtsov et al. [15, 16] studied the mechanical difference between the submicron titanium alloy and the microcrystalline titanium alloy at room and high temperature. It is pointed out that the submicron structure can improve the strength and fatigue limit. Gupta et al. [17] analyzed the strain hardening behavior of the Ti-6Al-4V sheet under a low strain rate and different heat treatment conditions. They found that the ultimate tensile strength increased with the increase of strain rate under all conditions. Guo et al. [18] discussed the relationship between heat treatment and the microstructure. The results show that the heat treatment can adjust the microstructure (equiaxed  $\alpha$  and lamellar  $\alpha$ ) characteristics and then affect the mechanical properties. The previous researches mainly focus on the deformation mechanism under uniaxial loading conditions. They seldom consider the material's

anisotropic behavior during the forming process. Since most Ti-6Al-4V components are processed by different methods, they are not subject to only one single direction of loading. The mechanical properties and the anisotropic behavior of Ti-6Al-4V need to be revealed.

Currently, the research on the anisotropy of titanium alloy has attracted the attention of scholars. Wahed et al. [19] studied the anisotropic effect on the superplastic mechanical properties of Ti-6Al-4V at low strain rates from 700 °C to 900 °C. The results show that the anisotropic behavior becomes weaker with the temperature increases. Ali et al. [20] considered that the texture of the  $\beta$  phase is the main reason for the anisotropic superplastic flow stress of the Ti-6Al-4V alloy sheet. Chen et al. [21] studied the anisotropic behavior of extruded Ti-6Al-4V-xB alloy and believed that the anisotropy was caused by the (0002)  $\alpha$  phase texture. In selective laser melting of the Ti-6Al-4V alloy, Yang et al. [22] found that the laser energy density would change the crystal orientation and lead to mechanical anisotropy. Besides, Li et al. [23] suggested that the cause of anisotropy of Ti-6Al-4V alloy was due to lack of fusion defects and  $\beta$  grain boundary  $\alpha$  colony in different orientations. Nakai et al. [24] found that twice heat treatment at 1273 K and 973 K could reduce the anisotropic behavior of the Ti9 alloy sheet. Wang et al. [25] rolled pure titanium with various routes (unidirectional, cross, and three directions) and different speeds. The results show that the anisotropic behavior of pure titanium rolled in three directions is the smallest. Yu et al. [26] analyzed the influence of dislocation and texture on the anisotropy of the TA5 titanium alloy sheet. They concluded that the basal plane texture is the main factor affecting the anisotropy. Zhu et al. [27] studied the TC11 alloy formed by additive manufacturing and found that annealing in the  $\beta$  phase field can significantly reduce the tensile anisotropic behavior.

The improvement of the anisotropic difference is significant for the actual production and application of titanium alloy parts. Although some researchers have investigated the anisotropy of Ti-6Al-4V alloy, there are relatively few systematic studies on the anisotropic flow characteristics, anisotropic microstructure evolution, and anisotropic fracture mechanism. Therefore, in this work, the hot flow behavior and anisotropic deformation mechanism of Ti-6Al-4V alloy are systematically studied by uniaxial

hot tensile tests and SEM-EBSD microstructure observation. The influence of orientation dispersion on phase transformation and softening behavior is discussed, and the anisotropic mechanism from yield to fracture of titanium alloy is revealed. This research will broaden the application of Ti-6Al-4V components in the industry.

## Materials and experiments

### Materials

The chemical composition of the Ti-6Al-4V alloy used in this study is given in Table 1. The alloy is a dual-phase alloy, in which the  $\alpha$  phase is HCP, and the  $\beta$  phase is BCC [13]. In order to reduce the internal stress caused by rolling, the sheet was annealed at 473 K for 2 h. The thickness of the cold-rolled sheet is 2 mm.

### Uniaxial hot tensile test

The static uniaxial tensile test was carried out at high temperatures to investigate the thermomechanical properties of Ti-6Al-4V alloy. The sheet was cut into a dog bone shape tensile sample, as shown in Fig. 1. Holes of  $\Phi$  10 are reserved at both ends of the non-calibration area to adapt the clamps. The size of the tensile sample is shown in Fig. 1a. The sheet is cut along the rolling direction (RD), 45° to the rolling direction and perpendicular to the rolling direction (TD), as shown in Fig. 1b. The test equipment is shown in Fig. 2. The test specimen is placed in a tubular heating furnace. The furnace temperature is monitored by connecting the nickel–chromium thermocouple to provide temperature feedback for the system. Once the temperature in the furnace is stable, the tensile test is carried out. All tests performed are shown in Table 2. In the first group, nine tests were carried out using RD specimens with the temperature at 923 K, 973 K, and 1023 K, strain rate at 0.001 s<sup>-1</sup>,

**Table 1** Chemical composition of Ti-6Al-4V titanium alloy (mass fraction)

Al	V	O	Fe	C	N	H	Ti
6.50	4.10	0.16	0.21	0.03	0.015	0.002	Bal

**Figure 1** Tensile specimen  
**a** Dimensions of tensile specimens; **b** Directions of specimens.

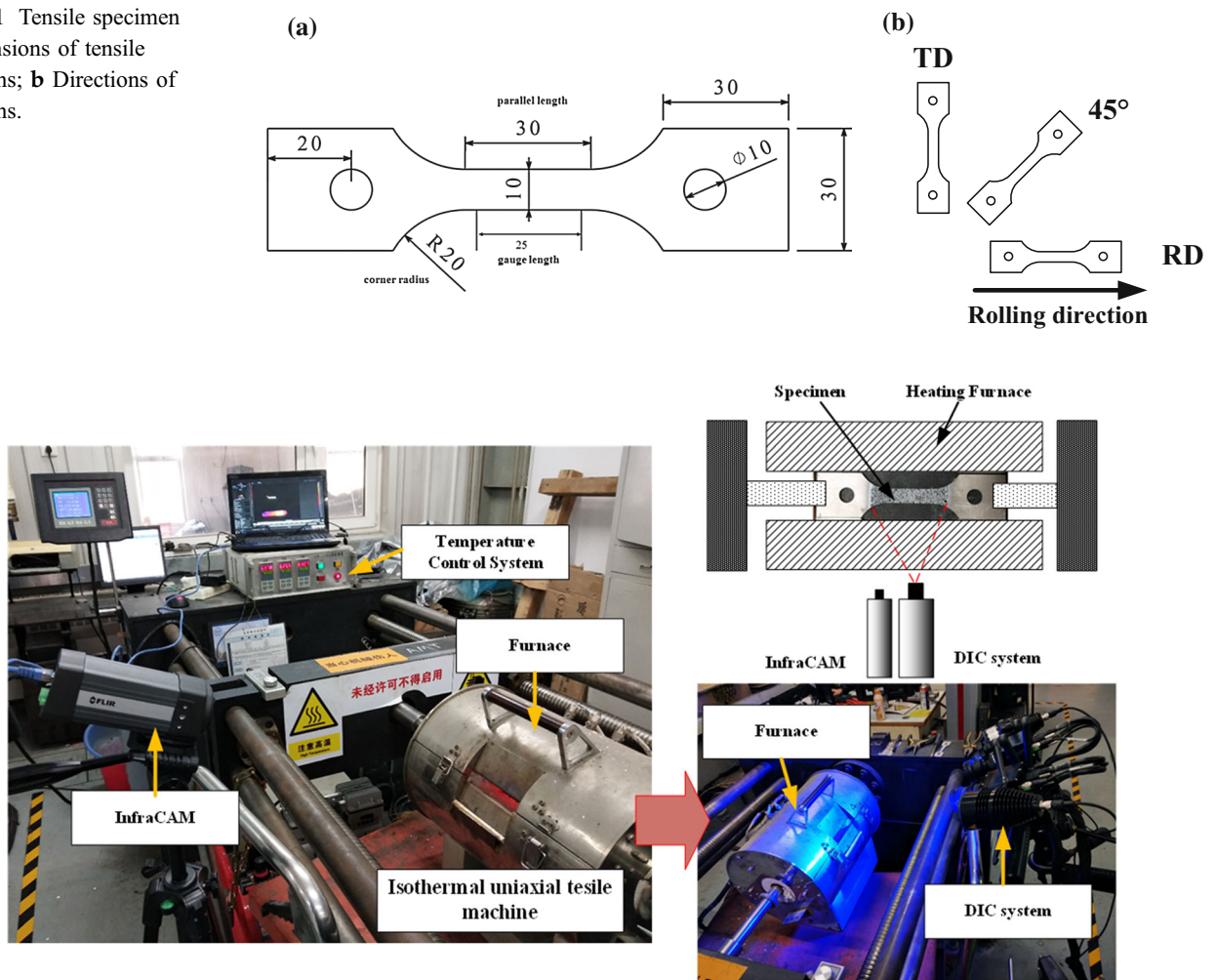


**Figure 2** Experimental equipment for uniaxial hot tensile test.

0.01 s<sup>-1</sup>, and 0.1 s<sup>-1</sup>, the heating rate is 5 °C/s. Once the sample is necked and broken, the high-temperature furnace will be opened to take out the sample for rapid cooling. In the second group, three 45° and three TD specimens were tested at 973 K to 1023 K and strain rates of 0.01 s<sup>-1</sup> to 0.1 s<sup>-1</sup>. The stress and strain fields were measured by the DIC system (GOM). Before the test, all specimens were uniformly sprayed with random speckle patterns, as shown in Fig. 2. Two high-resolution cameras were used to photograph the 3D position change of the spot at 20 Hz. Then the strain field of the deformed specimen was calculated by using commercial DIC software GOM Aramis.

### Characterization of microstructure

The microstructure and texture of the test specimens are characterized by scanning electron microscopy (SEM) and electron backscatter diffraction (EBSD). The Vega 3 XMU (LaB6) field emission SEM (TESCAN) was used in the experimental system equipped with Oxford / Nordlys EBSD detection system. Since the Ti-6Al-4V is a dual-phase alloy, EBSD samples should be prepared carefully to obtain high recognition patterns. Firstly, the stretched sample is cut into 7\*7\*1.3 mm samples. Then, the samples are ground to 1.1 mm thick with 800 sandpaper. After ground, the samples are mechanically polished to 7\*7\*1 mm with 1200 sandpaper. Then the polished samples were placed in ethanol for ultrasonic cleaning. At last, the argon-ion polishing was carried out at 3 kV voltage



**Table 2** Information of all test groups

Group	Direction	Temperature	Strain rate
Group 1	RD	923 K	0.1 s <sup>-1</sup>
	RD	923 K	0.01 s <sup>-1</sup>
	RD	923 K	0.001 s <sup>-1</sup>
	RD	973 K	0.1 s <sup>-1</sup>
	RD	973 K	0.01 s <sup>-1</sup>
	RD	973 K	0.001 s <sup>-1</sup>
	RD	1023 K	0.1 s <sup>-1</sup>
	RD	1023 K	0.01 s <sup>-1</sup>
	RD	1023 K	0.001 s <sup>-1</sup>
Group 2	45°	973 K	0.1 s <sup>-1</sup>
	45°	973 K	0.01 s <sup>-1</sup>
	45°	1023 K	0.1 s <sup>-1</sup>
	TD	973 K	0.1 s <sup>-1</sup>
	TD	973 K	0.01 s <sup>-1</sup>
	TD	1023 K	0.1 s <sup>-1</sup>

for 4 h. The scanning area is 769 μm\*577 μm, and the step size is 0.15 μm.

To investigate the anisotropic fracture mechanism of Ti-6Al-4V alloy at high temperature, the fracture surface of the tested specimen was observed by SEM. The fracture samples (parallel to the fracture direction) were cut by wire cutting. Then they were immersed in alcohol for two minutes to remove the oil and impurities. They were corroded with 2% nitrate solution for the 30 s. The cleaned and dried fracture samples were placed on the workbench for SEM observation. The fracture morphologies were obtained at 500–5000 magnification.

## Results and discussion

### Hot flow behavior

#### *Experimental results of group 1*

Each test was performed three times, and the data were averaged. Under the RD loading conditions, the stress–strain curves (experimental results of Group 1) are shown in Fig. 3. Among them, The 9 test results are compared in two patterns. As shown in Fig. 3a–c, one compares different strain rates under the same temperature at 923, 973, and 1023 K, respectively. The other compares different temperatures under the

same strain rate at 0.1 s<sup>-1</sup>, 0.01 s<sup>-1</sup>, and 0.001 s<sup>-1</sup>, as shown in Fig. 3d–f.

As shown in Fig. 3, the flow stress is greatly affected by temperature and strain rate, which verifies the conclusions of previous studies. At the beginning of the deformation, all the experimental curves rise rapidly because of the rapid accumulation of dislocations. It appears linear elasticity. When the stress exceeds the yield stress, the curve shows non-linear properties. In the plastic deformation stage, the material appears a softening phenomenon. With the stretching going on, the stacking of dislocations leads to the uneven distribution of dislocations. The specimen begins to be necking down [28–30]. When the shear stress exceeds the critical shear stress, the damage cracks appear at the edge of the specimen. The crack proliferates along a certain angle until the specimen breaks. During this process, the true stress decreases quickly.

#### *Effects of strain rate*

As shown in Fig. 3a–c, the flow stress increases with the strain rate at each deformation temperature. The main reason is that the high strain rate increases the deformation storage energy of the metal [31, 32], making the plastic deformation in the deforming body unable to be completed. Figure 4 shows the effect of strain rate on yield strength and tensile strength. When the temperature is constant, the yield strength and the tensile strength increase with the strain rate. In the strain rate range from 0.001 s<sup>-1</sup> to 0.1 s<sup>-1</sup>, the yield strength difference of Ti-6Al-4V alloy is about 260 MPa. The maximum tensile strength difference is 315 MPa, and the minimum difference is 226 MPa, which verified that the Ti-6Al-4V alloy is a strain rate-sensitive material. Besides, with the increase of strain rate, the increasing range of flow stress is more extensive due to the rise of plastic deformation per unit time, which requires more dislocations movement [33–35]. As a result, the internal distortion is intensified. The dislocations are entangled to form a cut step [36], making the slip and diffusion of dislocations more difficult. Insufficient dynamic recrystallization (DRX) and untimely dynamic recovery (DRV) can also increase flow stress.

Figure 4c shows the effect of strain rate on elongation. It can be found that the elongation increases with the decrease of strain rate at each temperature.

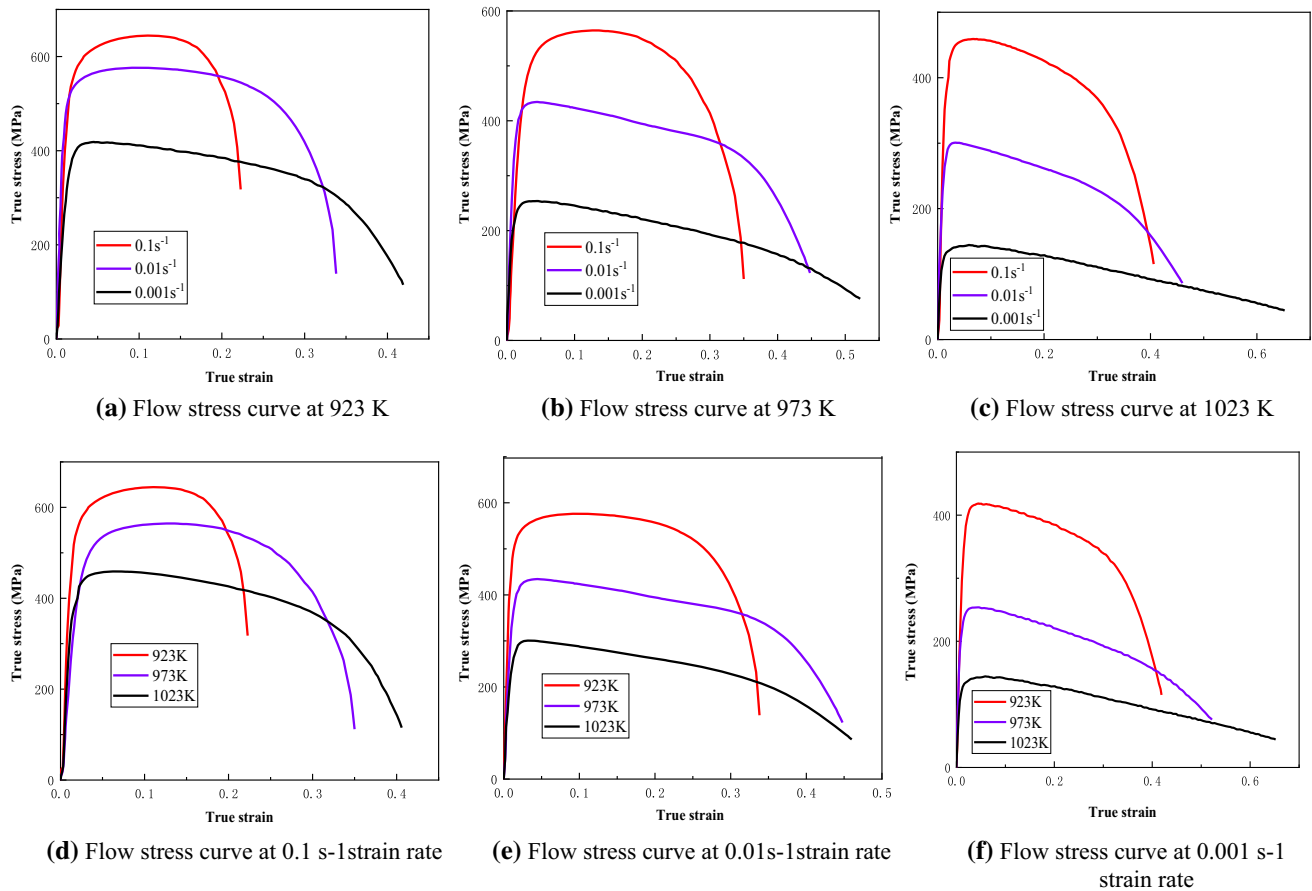


**Figure 3** Flow stress curves of hot tensile tests.

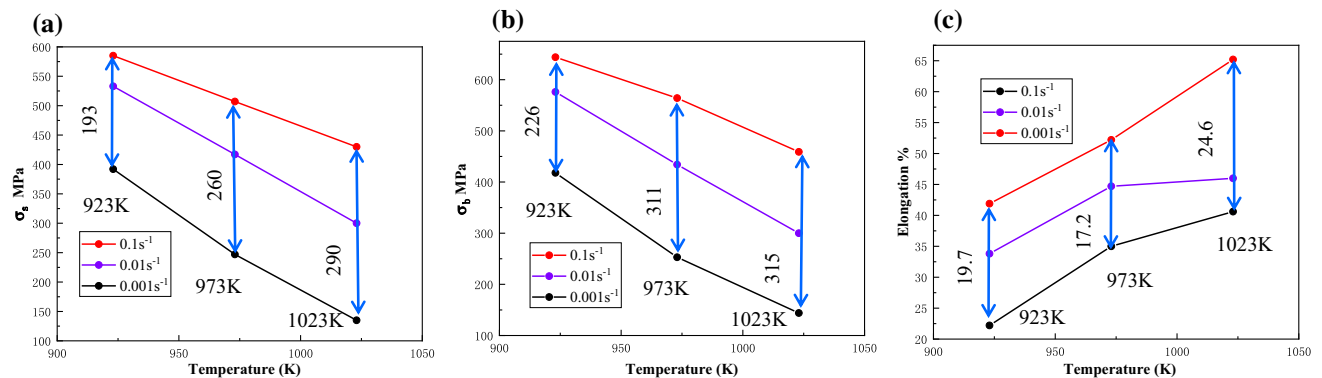


**Figure 4** Mechanical properties under different conditions: **a** yield strength, **b** tensile strength, and **c** elongation (%).

As the strain rate decreases, the dislocation density decreases, and the dislocation increment rate decreases [37], which increases the required degree of deformation to reach the maximum stress. The low strain rate provides more time for DRX and DRV of grains during deformation, generating more DRX and DRV, improving its ductility [38]. Therefore, the

decrease of strain rate will increase the ductility of Ti-6Al-4V alloy.

#### Effects of temperature

As shown in Fig. 3d–f, the flow stress of Ti-6Al-4V alloy decreases with the increase of deformation temperature at each strain rate. Figure 4 shows the

influence of temperature on yield strength and tensile strength. Since the Ti-6Al-4V is a temperature-sensitive material, the maximum and minimum differences of yield strength are 280 and 80 MPa between 923 and 1023 K. For tensile strength, these differences change to 270 and 100 MPa. The changing trend of yield strength and tensile strength is almost the same, and they are both decrease with the increase of temperature. With the increase of temperature, the thermal activation mechanism of this effect is enhanced. The average absorbed kinetic energy of each atom increases, which results in the amplitude of atomic vibration increases. Besides, the required Gibbs free energy for pinning dislocations to cross the energy barrier is reduced under the thermal activation mechanism, so the mobility of dislocations, vacancies, and slip systems increases [39–41], which enhances the metal plasticity and reduces the strength. Meanwhile, the temperature increase accelerates the DRV and DRX of the plastically deformed grains and enhances the softening effect [42]. The combined effect of these factors reduces the critical resolved shear stress, resulting in a decrease in the flow stress of the alloy.

Figure 4c shows the effect of deformation temperature on the elongation from 923 to 1023 K. Since the  $\alpha$  phase in Ti-6Al-4V alloy is the close-packed hexagonal structure, the number of movable slip systems in the hexagonal lattice will increase with temperature [12]. Under the high-temperature condition, the dislocation slip mechanism dominates the deformation [11], making deformation easier than the room temperature condition. Therefore, the increase of temperature improves the alloy's plasticity and elongation significantly.

## Anisotropic mechanical behavior

### Experimental results of group 2

Figure 5 shows the stress–strain curves of Group 2. When the temperature and strain rate is the same, the yield strength, flow stress, and elongation vary significantly under different loading path. It shows remarkable anisotropy. Many factors can cause material anisotropy, such as the actuation condition of the slip systems, initial texture, DRV, and DRX. They will be discussed in Sect. 3.3.

### Analysis of anisotropic yield strength

Figure 6 shows the anisotropic yield strength under different loading paths. It is noticed that the yield strength of the 45° loading is always at the bottom of the valley. Especially at 973 K-0.1 s<sup>-1</sup>, the yield strength difference between the TD direction and the 45° direction is 61 MPa (more than 10% of yield strength), seriously affecting the forming quality. With the decrease of temperature or strain rate, the difference in yield strength decreases greatly. The change of yield strength in the RD and the 45° directions is smaller than that in the TD direction, which shows that the yield strength in the TD direction is more sensitive to temperature and strain rate than the others.

### Analysis of anisotropic elongation

Temperature and strain rate can significantly affect the elongation of Ti-6Al-4V, which has been proved in the previous chapter. Figure 7 shows the change of elongation under different loading paths. At 973 K-

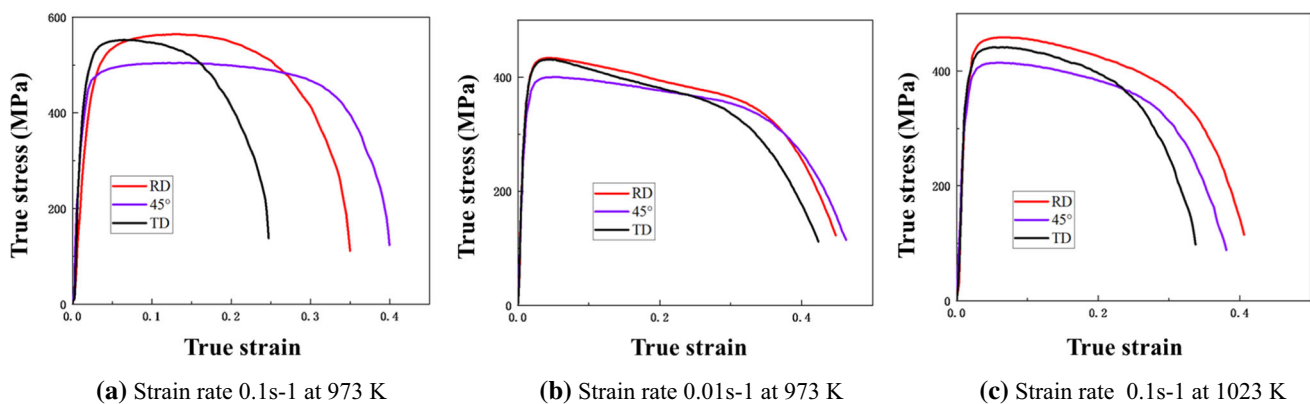


**Figure 5** Flow stress curves in different loading paths.

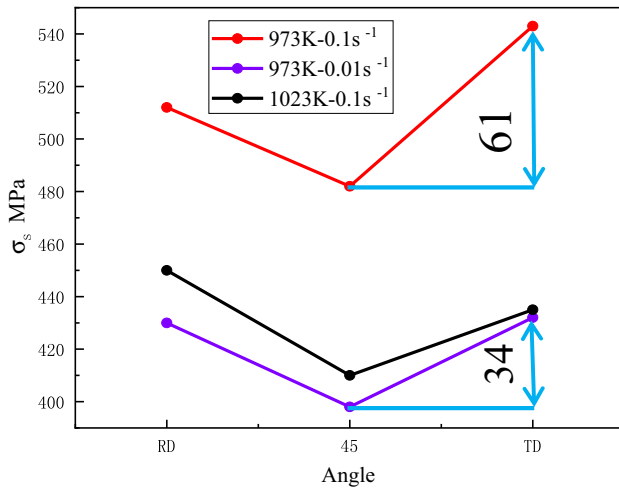


**Figure 6** Anisotropic yield strength.

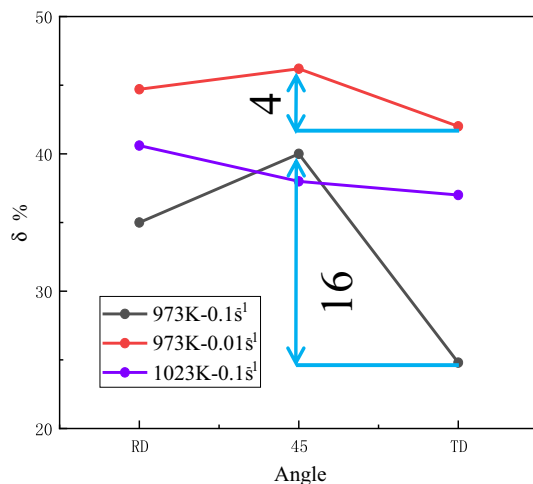


**Figure 7** Effect of anisotropy on elongation.

$0.1 \text{ s}^{-1}$ , the difference of elongation between the TD and the  $45^\circ$  is about 16%, seriously affecting the forming quality. With the decrease of strain rate or the increase of temperature, the elongation increases greatly under the TD direction loading, which reduces the gap to the RD and the  $45^\circ$  directions. However, when the temperature increases, the elongation of the  $45^\circ$  direction is lower than that of the RD direction. The change of grain orientation resulting in the incongruity of grain deformation and the decrease of elongation.

In the forming process, it is expected that the anisotropy of metal is insignificant, or the loading path with good forming quality can be used to achieve high-quality plastic forming. The experimental results show that the  $45^\circ$  loading direction is the most suitable loading path for the hot forming of titanium

alloy due to its good elongation and low yield strength. Besides, the anisotropy can be reduced by increasing the temperature or decreasing the strain rate.

### Anisotropic deformation mechanism at $973 \text{ K}-0.1 \text{ s}^{-1}$

#### Analysis of texture

The SEM-EBSD results are used to analyze the anisotropic mechanism. In Fig. 8, PD represents the perpendicular direction, and ND represents the normal direction. According to the IPF figures, the grain orientations and microstructures differ significantly after loading in different directions. The results show that the loading direction has a great influence on the microstructure evolution. Figure 8a shows the IPF figure of the material's initial state and the pole figures of (0001), (11–20), and (10–10) of  $\alpha$  phase. It can be seen that the orientation of the basal plane (0001) of the crystal is mainly concentrated in the TD direction, so the texture type is a typical T-type texture, and the extreme density is as high as 32.62. However, the pyramidal (11–20) and prismatic (10–10) pole figures show weakening texture. Their orientations are scattered, which shows that the angle between the c-axis and the grain loading direction is different, leading to the different initial difficulty for the basal slip and prismatic slip. The texture changes significantly after hot tension, as shown in Fig. 8b–d. Under the RD loading conditions, the T-type texture gradually disappeared. Meanwhile, the texture on the (10–10) crystal plane (max = 10.25) appeared. The results show that with the rotation and deformation of the grains, the orientation of grains tends to (10–10). Under the  $45^\circ$  and TD direction loading conditions, the (0001) crystal plane has multiple texture orientations with the maximum values of 9.16 and 10.47, respectively. Due to the influence of thermal activation, the strength of the texture decreases significantly after stretching in all directions. The grain rotation, phase transformation, DRV, and DRX will lead to the random crystallographic orientation of the material. When the material is deformed, the weaker texture means a more extensive grain orientation distribution [43]. With the progress of deformation, the grain orientation will be more suitable for the deformation of the material. The elongation rate of the material is improved. The phenomenon of



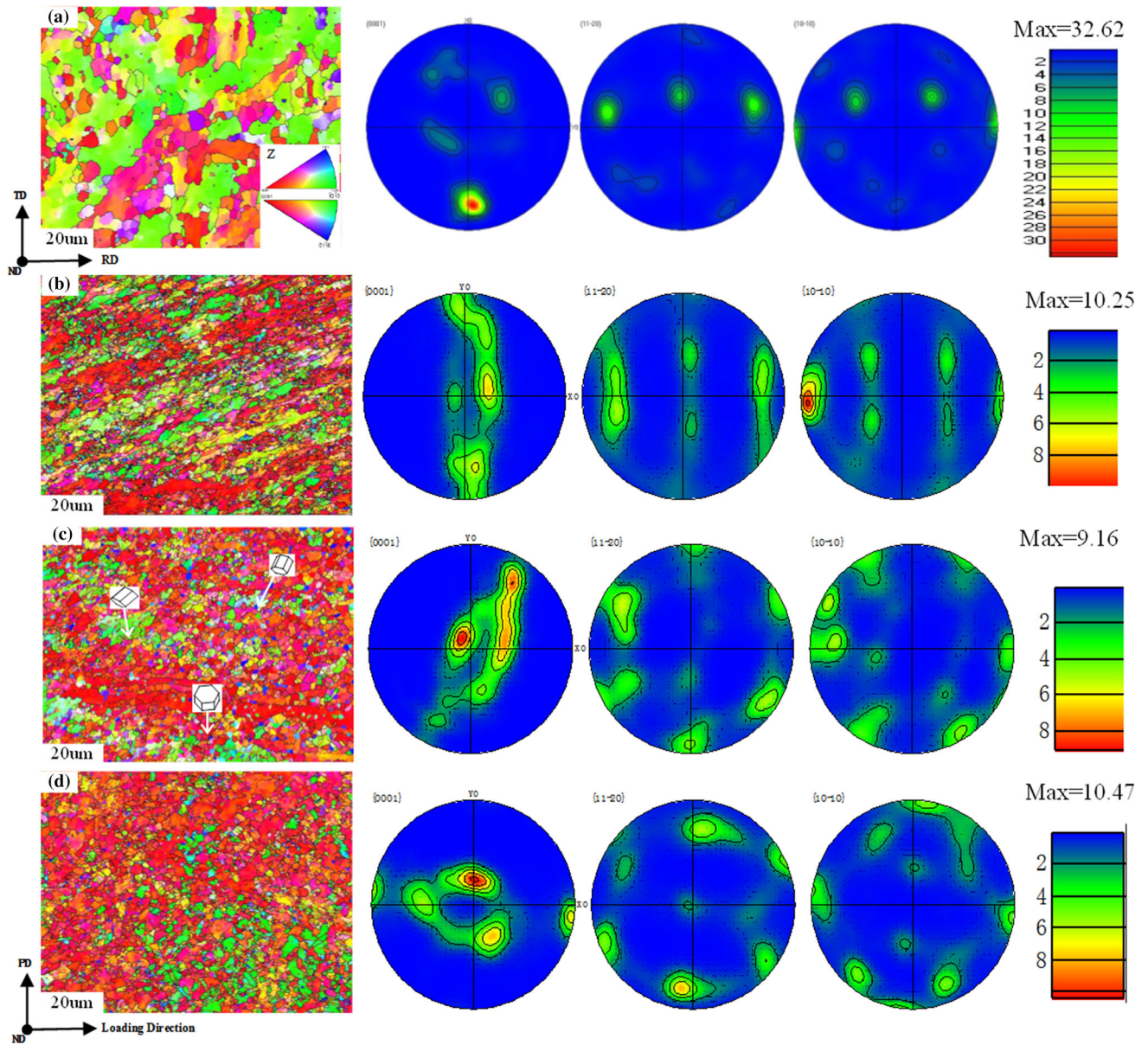


**Figure 8** EBSD maps and pole figures: a Initial; b RD; c 45°; d TD.

texture weakening is the most significant in the 45° direction, and the plasticity is also the best.

*Analysis of Schmid factor*

The activation of the slip system is positively correlated with the value of the Schmid factor. The prismatic and basal slips are relatively easy to activate at high-temperature loading conditions because of their low critical resolved shear stress (CRSS) levels [45]. For Ti-6Al-4V at room temperature, the CRSS ratio of basal and prismatic is 1:1.06 [44]. Their active

conditions are similar. At 728 K, the CRSS ratio of the basal and prismatic slip systems changes to 1:1.38 [45]. The basal slip is more accessible to activate than prismatic slip. However, at 1088–1228 K, when the temperature approaches the phase transformation temperature, the situation has reversed, the CRSS ratio changes to 1:0.7 [46]. The slip system varies with the crystal structure, influencing the value of CRSS.

The yield strength shows pronounced anisotropy so that the texture will affect the Schmid factor of the slip system. The calculation formula of the Schmid factor is as follows:

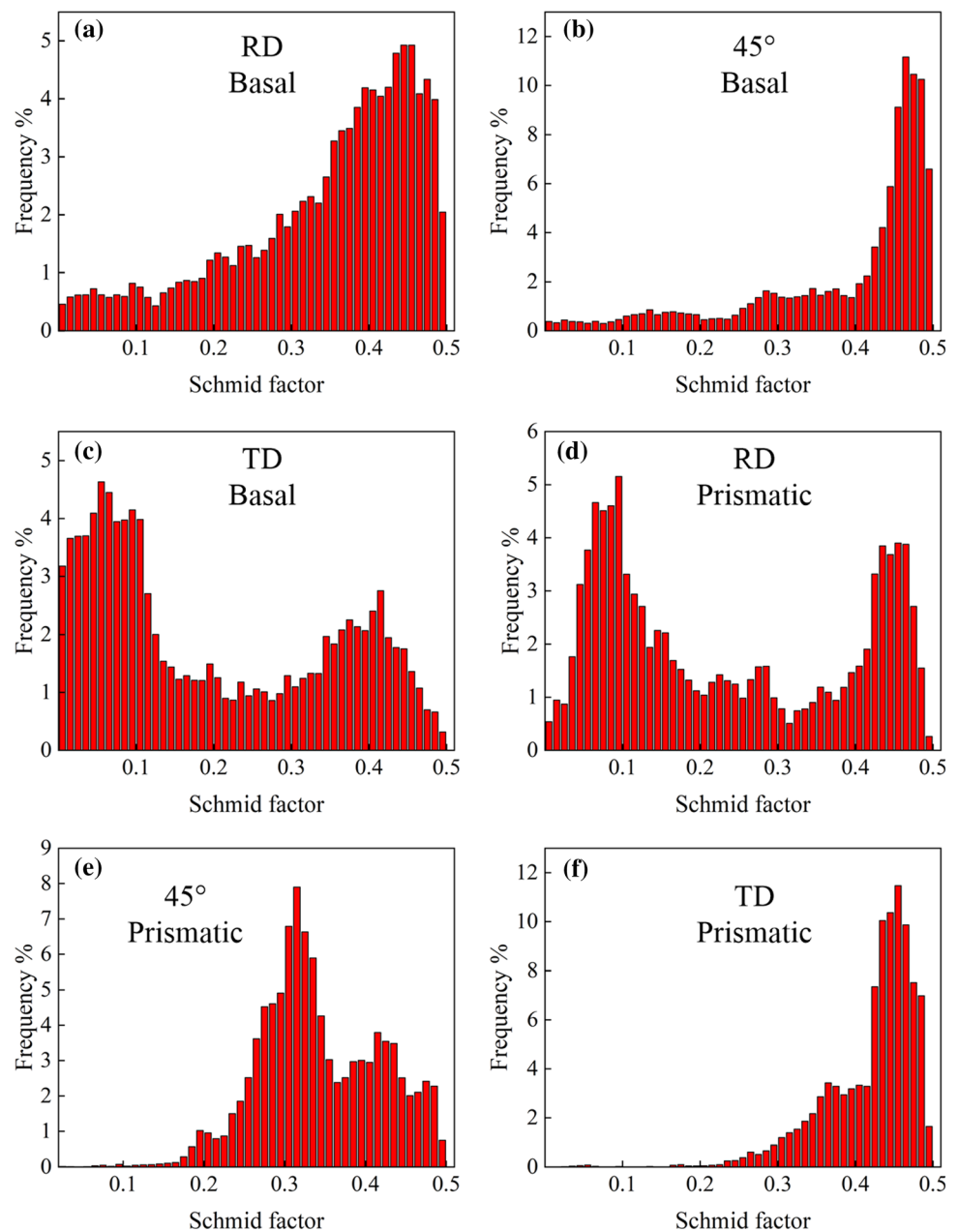
$$m = \cos \phi \cdot \cos \lambda \quad (1)$$

where  $\phi$  is the angle between the loading direction and the normal of slip plane, and  $\lambda$  refers to the angle between the loading direction and the slip direction.

The data of RD, 45°, and TD are analyzed by channel 5 software. Figure 9a–c shows the initial state of the Schmid factor for the (0001)[11–20] basal slip system in different directions. The distribution of the Schmid factor in the RD loading direction between 0–0.5 shows a monotonic increasing trend, and 65% of Schmid factors are between 0.25–0.5. Under 45°

loading, the values of most Schmid factors are between 0.4 and 0.5, and the slip system is the easiest to start. Due to the effect of texture, the normal stress direction of TD direction is almost parallel to the c-axis of the grain, so the value of most Schmid factors is between 0–0.25. Through the Schmid factor analysis of the basal slip system, the yield strength of the TD direction is the highest. The 45° directional yield strength is the lowest, which is consistent with the experimental results. Figure 9d–f shows the initial state of the Schmid factor for (10–10)[11–20] prismatic slip system in different directions. The

**Figure 9** The distribution of Schmid factor in different directions of initial state: **a–c** basal slip system; **d–f** prismatic slip system.

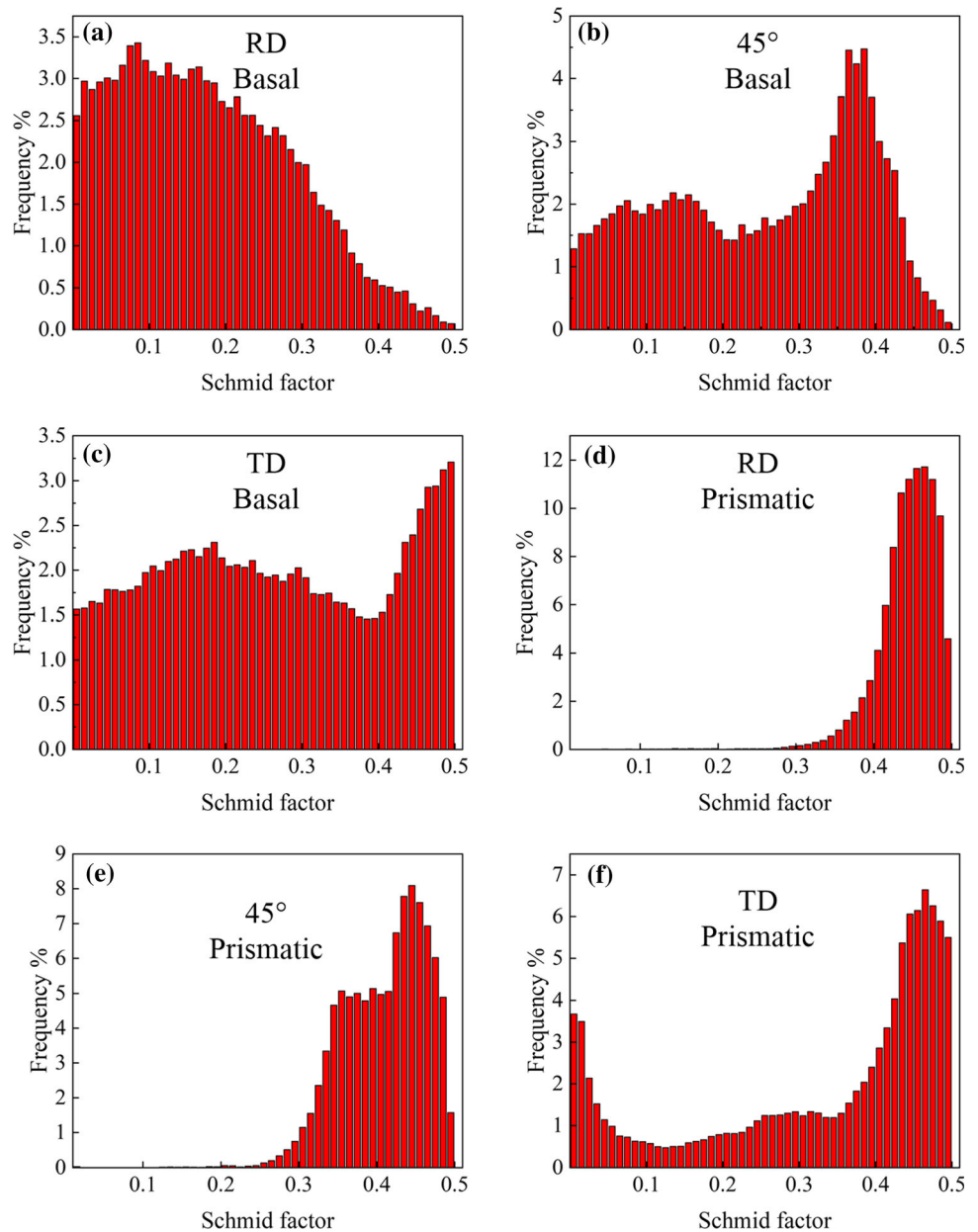


Schmid factor of prismatic slip system loaded in RD direction shows a bimodal distribution, and about 55% of Schmid factor is between 0–0.25. The Schmid factor is between 0.25–0.5 in 45° and TD directions, and the slip system is relatively easy to start. The yield strength in the direction of TD is the highest, and the yield strength in the direction of 45° is the lowest through the analysis of basal and prismatic slip systems. The average Schmid factors of the initial state for the basal and prismatic are calculated as 0.31 and 0.33, respectively, indicating that their active

conditions are similar, which is consistent with the conclusion in Reference [44].

After loading in different directions, the Schmid factor of the basal and prismatic slip systems are shown in Fig. 10. In the RD loading direction, the Schmid factor of the basal slip system is significantly reduced. About 75% of the Schmid factor is between 0–0.25. The Schmid factor of the prismatic slip system increased greatly, and the distribution was mainly between 0.4 and 0.5. The strong texture of the (0001) crystal plane under RD loading is weakened with the rotation of the grains. At 45° and TD direction, the

**Figure 10** The distribution of Schmid factor after tension in different directions: **a–c** basal slip system; **d–f** prismatic slip system.





Schmid factor of the basal slip system is reduced and distributed evenly between 0–0.5. The Schmid factor of the prismatic slip system under 45° loading is small, while the Schmid factor of the prismatic slip system under TD loading slightly decreases. The tensile strength of the TD direction is the highest by Schmid factor analysis after deformation. The lowest tensile strength is the 45° direction, which is in agreement with the test results. The average Schmid factors of the basal and prismatic after loading are calculated as 0.23 and 0.39, respectively. The experimental results show that the activity of the prismatic slip system is higher than that of the basal slip system after high temperatures loading, which is consistent with the conclusion in Reference [46]. The Schmid factor of the basal and prismatic slip system changes significantly before and after deformation.

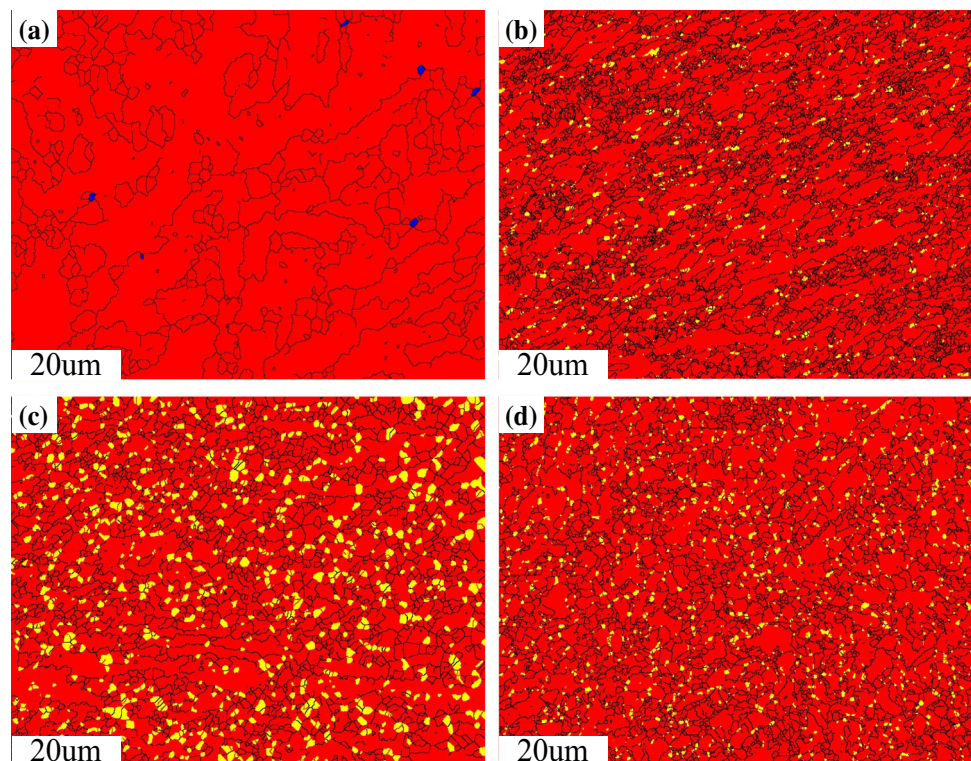
For Ti-6Al-4V, from room temperature to around 728 K, the basal slip is more active than the prismatic slip as the temperature increases. However, as the temperature approaches the phase transformation temperature, the situation reverses, and the prismatic slip system becomes easier to activate.

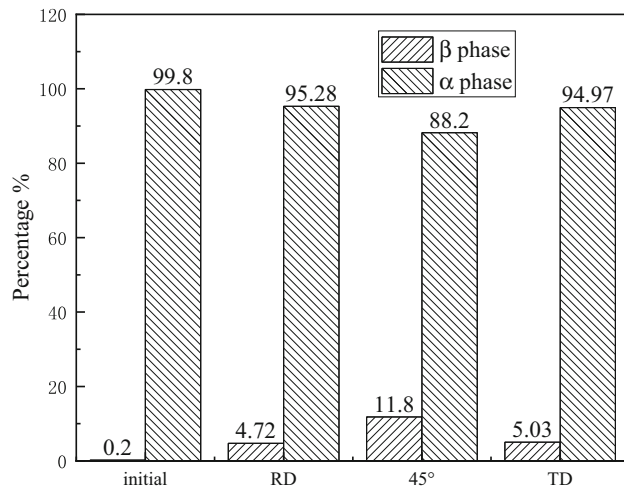
### Analysis of phase transformation

Figure 11 shows the distribution of two phases in the initial state and loading in different directions. The soft  $\beta$  phase is always uniformly distributed around the hard  $\alpha$  phase when loading from any direction. The  $\beta$  phase is minimal (0.2%) in the initial state. Since the phase transformation occurred during the loading process, the  $\beta$  phase ratio reached around 5% in RD and TD loading conditions. However, the phase transformation behavior increases significantly after 45° loading. The proportion of the  $\beta$  phase reaches 11.8%, as shown in Fig. 12.

Under the same temperature and strain rate, the difference of phase transformation behavior can be attributed to the texture of the {0001} crystal plane. As mentioned in 3.3.2, the Schmid factor of the slip system is different due to the texture. In the 45° direction, the Schmid factor reaches the maximum, and the number of dislocations is large. Dislocation density increases due to the effect of grain boundary in the process of slip. The growth of dislocation density leads to a large amount of deformation storage energy, making it easier to obtain the critical energy of phase transformation. Furthermore, it accelerates the change of crystal structure [42].

**Figure 11** Two phase distribution: **a** initial state (Red and blue indicate  $\alpha$  phase and  $\beta$  phase); **b** RD; **c** 45°; **d** TD (Red and gold indicate  $\alpha$  phase and  $\beta$  phase).





**Figure 12** Two-phase ratio of initial and different loading directions.

The change of grain orientation is the largest after 45° loading, as shown in Fig. 8. The different angle between the c-axis and the normal stress of the preferred orientation grains leads to the grains' different rotation. The colony of grains with the same orientation in the 45° direction is weaker than in the RD and TD directions. Its orientation dispersion is the largest. When dislocations slip to the grain boundary and encounter grains with different orientations, the grain boundary will hinder the movement of dislocations, increase dislocation density, and make phase transformation easier.

### Analysis of DRV and DRX

From the stress–strain curve of Fig. 5a, it is noticed that there is apparent softening behavior and the flow stress shows remarkable anisotropy. Dynamic recovery (DRV) and dynamic recrystallization (DRX) are the main reasons for the softening behavior of Ti-6Al-4V titanium alloy at high temperatures [47, 48]. DRV and DRX reduce the defects caused by dislocation slip and increase the elongation of the metal. Figure 13 shows DRV and DRX under different loading directions. Different DRX and DRV behaviors are produced due to texture. In Fig. 13, PD represents the perpendicular direction, and ND represents the normal direction. The grains with orientation differences less than 2° are marked red, which represents the deformed grains. During hot deformation, subgrain boundaries will appear in the grain due to DRV. The grains with 2–15 degrees of orientation

differences are marked yellow, which represents the substructure. With the progress of deformation, the small-angle grain boundary rotates continuously to form a large-angle grain boundary. The grains with an orientation difference above 15° are marked by blue, representing recrystallized grains [48, 49]. During hot deformation, dislocations will enter the grain boundary and form a series of dislocation substructures to reduce stress concentration. Subsequently, the dislocation substructure gradually transformed into a high-angle grain boundary, producing new DRX grains [42].

The DRX and DRV behaviors of  $\alpha$  and  $\beta$  phases are further analyzed. Figure 14 shows the DRV and DRX ratios of the  $\alpha$  phase under different loading directions. The ratios of DRX in RD, 45°, and TD directions are 4%, 0.5%, and 1.8%. The proportion of DRX is small in the  $\alpha$  phase. Since there is a large area of grains with the same or similar orientations in the RD and TD directions, the dislocations between these  $\alpha$  phase grains are more likely to enter the grain boundary and cause DRX behavior than the 45°. The proportion of DRV in 45° direction reaches 40.2%. The orientation dispersion of tensile grains in the 45° direction is the largest. The dislocations are not easy to enter the grain boundaries during the sliding process, resulting in many DRV grains. Besides, the rotation of grains leads to an increase in the number of slip systems, making the deformation uniform. In this case, DRV is more likely to occur than DRX. The DRV ratio of the  $\alpha$  phase is more prominent than that of DRX, so the softening caused by the  $\alpha$  phase is mainly DRV.

Figure 15 shows the ratio of DRV and DRX in the  $\beta$  phase. The DRV and DRX ratios of the  $\beta$  phase are much larger than that of the  $\alpha$  phase. There are many  $\beta$  phase slip systems produced by phase transformation, which makes the deformation easier. In the range of RD-45°-TD, the changing trend of DRV and DRX is consistent with  $\alpha$ . The RD and TD loading caused orientation difference of phase transformation grains is slight, which is still quite different with the 45° loading. It can be inferred that the orientation dispersion of the  $\beta$  phase generated by phase transformation depends on the orientation dispersion of the  $\alpha$  phase.

Based on the proportions of the two phases in Fig. 12 and the DRV and DRX proportions of the two phases in Figs. 14 and 15, the sum of the DRV and DRX proportions in the two phases can be calculated,



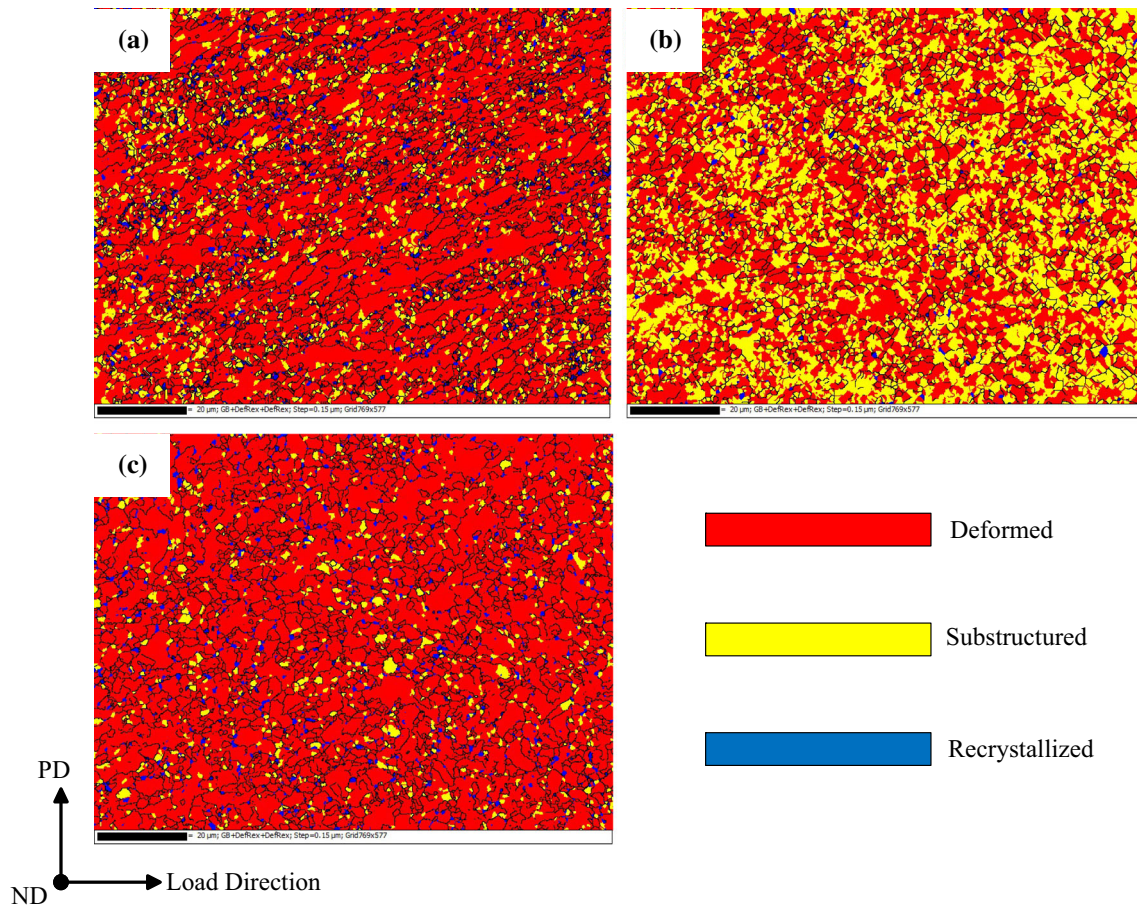


**Figure 13** Distribution of DRX, DRV and deformation in different loading directions: **a** RD; **b** 45°; **c** TD.

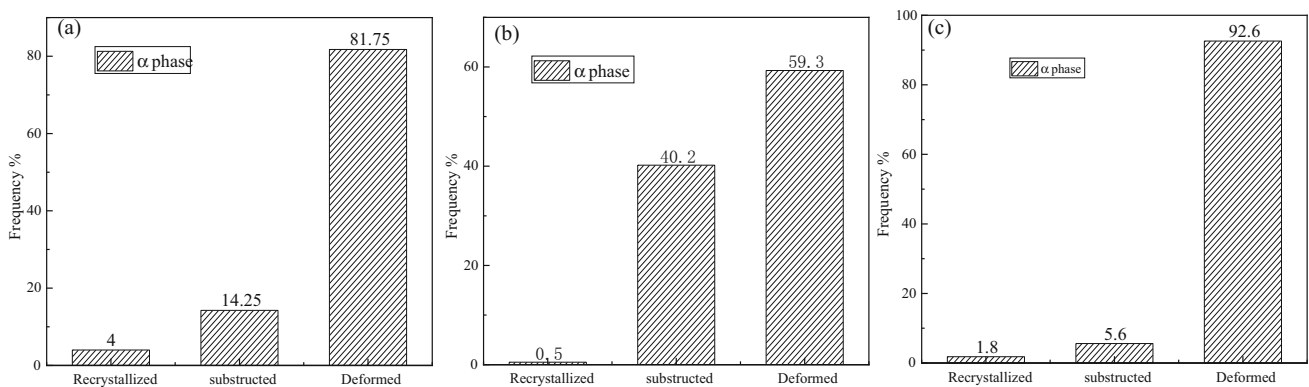


**Figure 14** DRV, DRX, and deformation structure distribution of  $\alpha$  phase at different angles: **a** RD; **b** 45°; **c** TD.

as shown in Fig. 16. The total DRX ratios generated by the two phases are 5.5%, 1.1%, and 4.1%, respectively. Comparing with DRV, there are relatively few grains produced by DRX, which has a limited effect on the softening behavior of the material. The nucleation/rotation of grain substructure is

dominant. Therefore, the primary mechanism affecting the softening behavior is DRV at 973 K.

In the process of plastic deformation, the increase of GND density will limit the movement of dislocations and reduce the content of DRV [50–52]. Reference [53] indicates that the value of Kernel Average Misorientation (KAM) could represent the density of

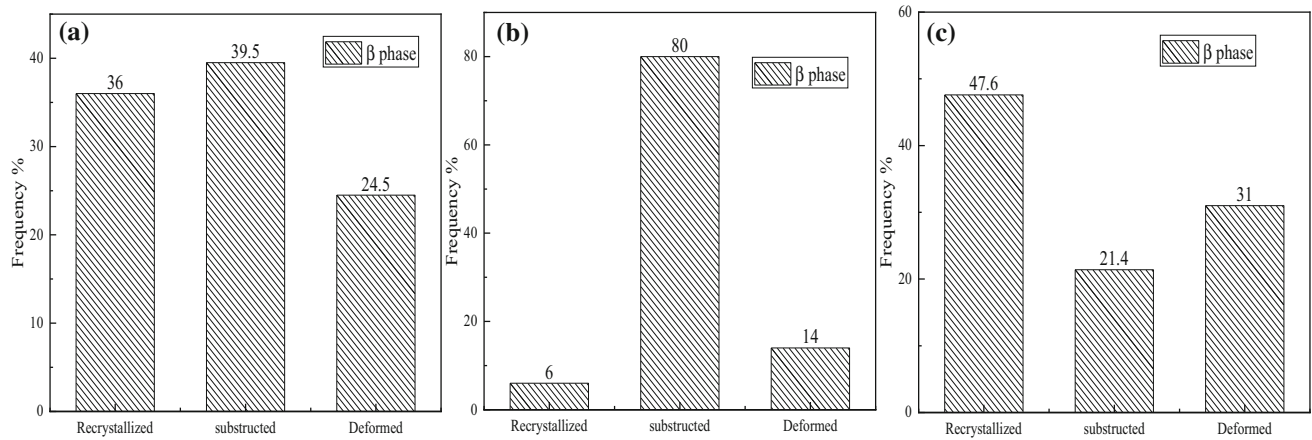


**Figure 15** DRV, DRX, and deformation structure distribution of  $\beta$  phase at different angles: **a** RD; **b** 45°; **c** TD.

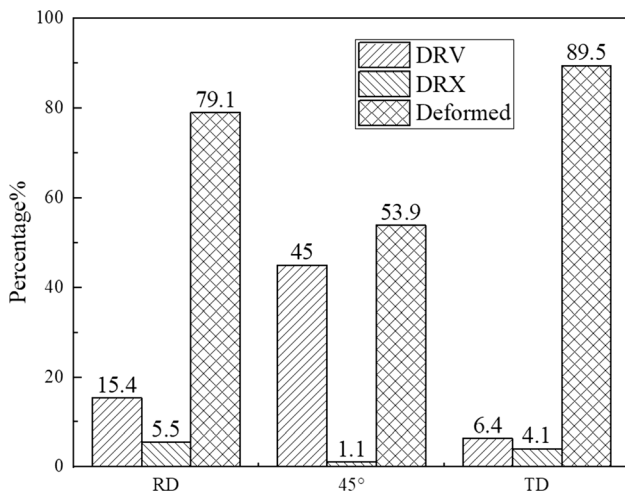


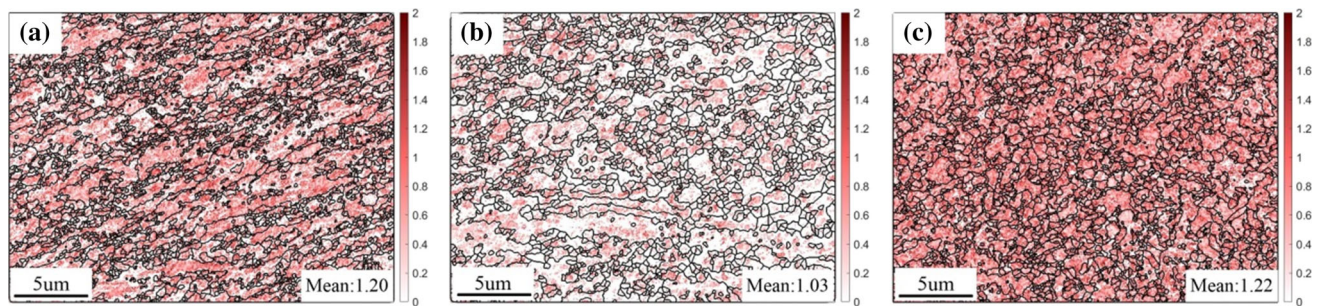
**Figure 16** DRV, DRX, and deformation structure distribution at different angles.

GND. Figure 17 shows that the average values of KAM at the 45°, RD, and TD are 1.03, 1.20, and 1.22, respectively. The KAM value at the TD is the highest. Since the basal plane orientation of the Ti-6Al-4V crystal is mainly concentrated in the TD direction, when it is loaded along the TD direction, its loading

direction is parallel to the c-axis, resulting in a higher GND value. Furthermore, GND will hinder the movement of dislocations, thereby limiting the occurrence of DRV and causing its softening phenomenon to be the weakest. The KAM value of the RD is lower than the TD because the loading direction is perpendicular to the c-axis. Its softening phenomenon is stronger than TD. The KAM value of the 45° sample is the minimum makes the softening phenomenon remarkable compared to the others. This phenomenon is because the Schmid factor's value is the largest, the slip system activity is the highest, so the GND is the lowest when loading at 45°. In summary, due to the different angles between the loading direction and the c-axis, the GND density is different, which results in a significant difference in the DRV of the material in different loading directions under high-temperature loading conditions.

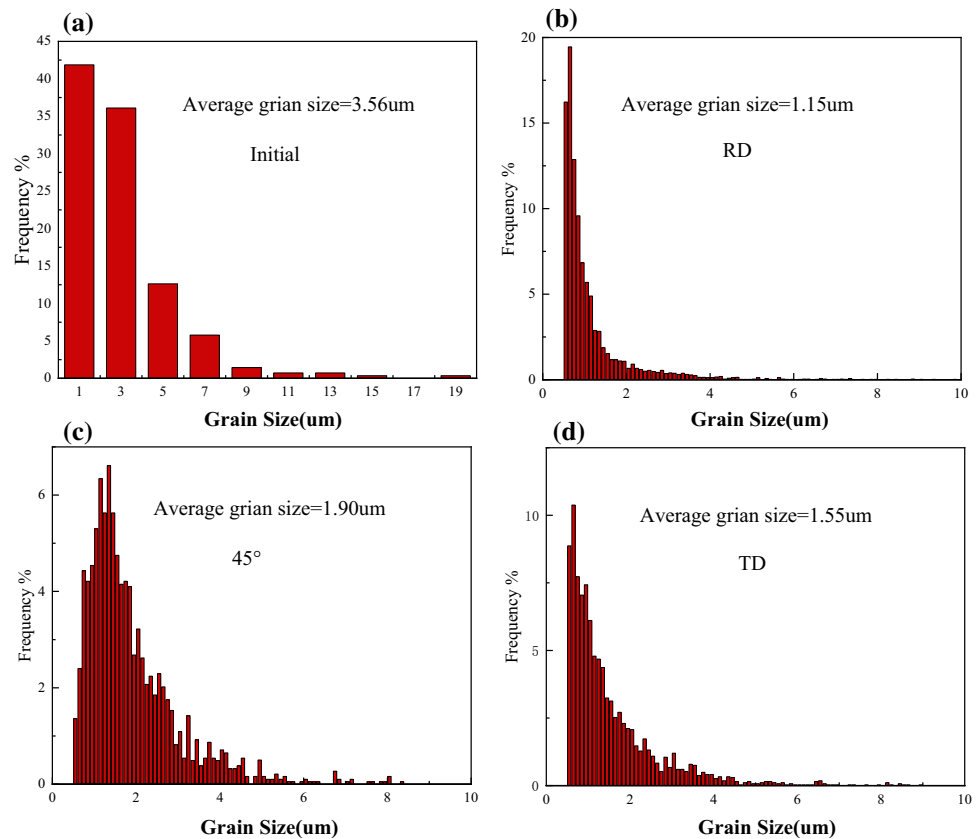
*Analysis of grain size*

Figure 18a shows the size of equiaxed grains in the initial state, with an average grain size of 3.56  $\mu\text{m}$ .



**Figure 17** KAM maps of the deformed samples **a** RD, **b** 45°, **c** TD.

**Figure 18** Grain size: a initial; b RD; c 45°; d TD.



After loading, the grains are elongated along the loading direction and refined to varying degrees, as shown in Fig. 8. Figure 18b shows the grain size distribution after loading in the RD direction, with an average grain size of 1.15  $\mu\text{m}$ , and the proportion of grains with different sizes varies greatly. The average grain size under 45° loading is 1.90  $\mu\text{m}$ , and the area fraction of grains with various sizes is balanced, as shown in Fig. 18c. It is found in Fig. 18d that the average grain size is 1.55  $\mu\text{m}$  when loading along the TD direction, and the grain content of different sizes is distributed between RD and TD. The grain size will become smaller after DRX, as shown in Fig. 13. The RD has the largest proportion of DRX, the average grain size is the smallest. Under 45° loading conditions, the ratio of DRV is much higher than that of DRX, so the average grain size is large. The average grain size is the largest, and the flow stress is the minimum during 45° tensile deformation.

#### *Analysis of fracture mechanism*

Figure 19 shows the fracture morphology of tensile samples at the strain rate of  $0.1 \text{ s}^{-1}$  at 973 K. Firstly,

for RD and 45° loading conditions, the cracks on the fracture surface are covered with many equiaxed dimples and tear edges, which shows a ductile fracture mechanism. Comparing the fracture morphology in the RD and 45°, it can be found that the 45° samples have more dimples, and the aggregation is stronger than the RD samples. Its tearing edges gather around the dimple. The dimples are few and scattered for the RD samples, and the sliding tear edges are more than that of 45°. The number, size, and depth of dimples under the 45° loading conditions are more extensive and profound than the RD. It has the performance of microvoid coalescence fractures in the 45° samples. In comparison, the RD samples have the characteristics of quasi-cleavage fractures. Then, the river patterns and many tear edges appeared on the fracture surface for TD loading. Besides, some shallow dimples are distributed at the crack edge in the  $5000\times$  magnified image. Therefore, the fracture mechanism for TD loading is a quasi-cleavage fracture. It can be seen from the SEM image that the cracks under TD loading are the most. The experimental results verified that 45° loading has the best plasticity and TD loading has the worst



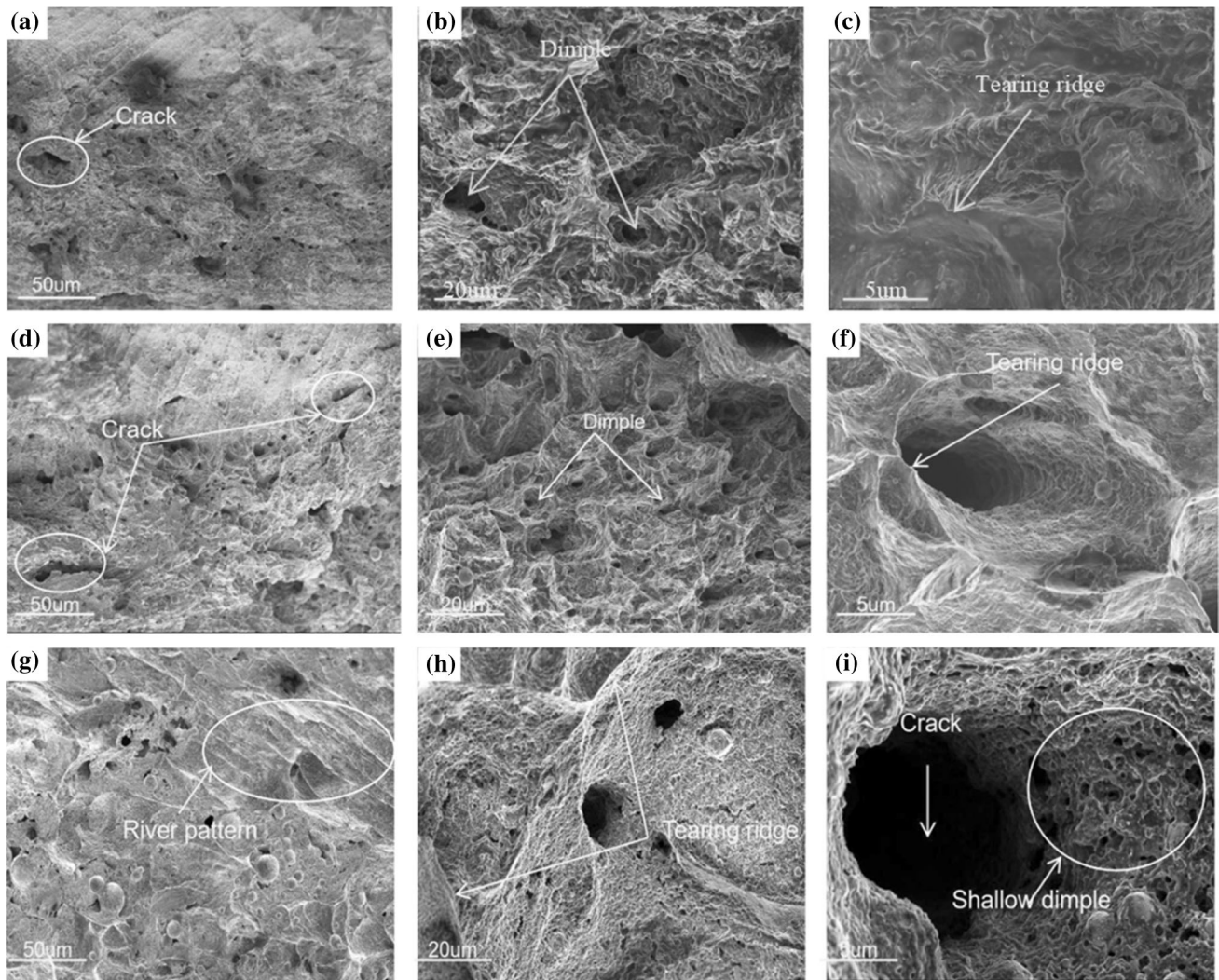


**Figure 19** Fracture under different loading directions: a–c RD; d–f 45°; g–i TD.

plasticity. During the deformation process of TD loading, the normal stress direction is nearly parallel to the c-axis of the crystal, and the Schmid factor is small. The basal and prismatic slip systems are difficult to start. It is easy to form cleavage crack at grain boundary due to the incongruity of deformation between grains. The grain boundary will hinder the forward propagation of cleavage crack. However, due to the rotation of grains in the TD loading direction, the orientation difference among the grains is small. The cleavage cracks continue to expand and finally tear the residual connection in the plastic section.

## Discussion

Through the above analysis, it can be seen that the factors causing the anisotropic behavior are multiple and closely related. However, the main factor is the T-type texture in the cold-rolled Ti-6Al-4V sheet. The initial loading stage is linearly elastic at high temperatures, and the elastic modulus difference is small under different loading paths. With the continuation of loading, the angle between the c-axis and normal stress of preferred oriented grains is different under different loading paths, resulting in different Schmid factors of slip system and anisotropy of yield strength. The DRV and DRX behaviors affect the grain size during the deformation process. By calculating the sum of the ratios of the two-phase DRV and DRX, the primary mechanism affecting the softening

behavior is DRV at 973 K. Under the influence of DRV, the grain size in the 45° direction is the largest. The flow stress at this stage is the lowest. After stable plastic deformation, necking occurs, and the stress decreases rapidly until fracture. In this process, both phase transformation and softening behavior affect elongation. The DRV and DRX reduce the defects caused by dislocation slip and greatly improve the elongation. After the metal fracture, the fracture mechanism is related to the Schmid factor and grain orientation. Firstly, it is difficult to start the slip system of preferred orientation grain under TD direction loading. The uncoordinated deformation between grains is easy to lead to crack initiation. Secondly, the grain orientation is concentrated in the TD direction, which promotes the intergranular crack expansion.

At high temperatures, the texture weakens differently after loading along different paths, indicating that hot deforming can reduce the anisotropy. When the temperature and strain rate is constant, the 45° loading has the lowest yield strength, the most balanced grain distribution, the most apparent texture weakening, and the largest elongation. Therefore, the loading along 45° direction can be selected in the production and processing. If anisotropy is unavoidable, the effect of anisotropy can be reduced by increasing temperature or decreasing strain rate.

## Conclusions

The anisotropic behavior and mechanical properties of cold-rolled Ti-6Al-4V alloy under high-temperature deformation are studied. In particular, the effect of texture on microstructure at 973 K-0.1 s<sup>-1</sup> is discussed. The conclusions are as follows:

1. The T-type texture of Ti-6Al-4V alloy in the  $\alpha$  phase is the main reason causing the anisotropy. Under high-temperature loading conditions, the texture weakening is noticeable, especially in the 45° loading path.
2. The mechanical properties of Ti-6Al-4V performed anisotropy significantly at 973 K-0.1 s<sup>-1</sup>. With the increase of temperature or the decrease of strain rate, the anisotropic characteristics can be weakened, and the forming quality of the Ti-6Al-4V alloy can be improved.
3. Under high-temperature loading conditions, the primary mechanism affecting the softening behavior is DRV. The different angles between the loading direction and the c-axis of the grains result in a significant difference in the DRV ratio.
4. The loading along 45° direction has the best forming quality. It can be selected in the processing of Ti-6Al-4V alloy.

## Declaration

## Conflict of interest

The authors declare that they have no known competing financial interests or personal relationships that could have appeared to influence the work reported in this paper.

## Ethical approval

This paper is new. Neither the entire paper nor any part of its content has been published or has been accepted elsewhere. It is not being submitted to any other journal as well.

## Acknowledgements

This work was supported by the National Natural Science Foundation of China (No.51805045) and Scientific and Technological Developing Scheme of Ji Lin Province (No. 20200401115GX)

## Availability of data and materials

The data during the current study are available from the corresponding author on reasonable request.

## References

- [1] Banerjee D, Williams JC (2013) Perspectives on titanium science and technology. *Acta Mater* 61(3):844–879
- [2] Lin YC, Tang Y, Zhang XY, Chen C, Yang H, Zhou KC (2019) Effects of solution temperature and cooling rate on



- microstructure and micro-hardness of a hot compressed Ti-6Al-4V alloy. *Vacuum*. 159:191–199.
- [3] Littlewood PD, Wilkinson AJ (2012). Geometrically necessary dislocation density distributions in cyclically deformed ti-6al-4v. *Acta Materialia*.
- [4] Abbasi SM, Momeni A, Lin YC, Jafarian HR (2016) Dynamic softening mechanism in ti-13v-11cr-3al beta ti alloy during hot compressive deformation. *Mater Sci Eng A* 665: 154–160.
- [5] Fan JK, Kou HC, Lai MJ Tang B, Chang H, Li JS (2013) Hot deformation mechanism and microstructure evolution of a new near  $\beta$  titanium alloy. *Mater Sci Eng A* 584:121–132
- [6] Balasundar I, Ravi KR, Raghu T (2017) On the high temperature deformation behaviour of titanium alloy bt3-1. *Mater Sci Eng A*, 684:135–145.
- [7] Ravindranadh B, Vemuri M (2018) Physically-based constitutive model for flow behavior of a ti-22al-25nb alloy at high strain rates. *J Alloy Compd* 762:842–848
- [8] Lee WS, Lin MT (1997) The effects of strain rate and temperature on the compressive deformation behaviour of ti-6al-4v alloy. *J Mater Process Technol* 71(2):235–246
- [9] Majorell A, Srivatsa S, Picu RC (2002). Mechanical behavior of ti-6al-4v at high and moderate temperatures—part i: experimental results. 326(2):297–305
- [10] Chen G, Ren C, Qin X, Li J (2015). Temperature dependent work hardening in ti-6al-4v alloy over large temperature and strain rate ranges: experiments and constitutive modeling. *Mater Des* 83:598–610.
- [11] Velay V, Matsumoto H, Vidal V, Chiba A (2016) Behavior modelling and microstructural evolutions of ti-6al-4v alloy under hot forming conditions. *Int J Mech Sci*, pp 108–109.
- [12] Ding R, Guo ZX, Wilson A (2002) Microstructural evolution of a ti-6al-4v alloy during thermomechanical processing. *Mater Sci Eng A* 327(2):233–245
- [13] Lee WS, Lin CF (1998) High-temperature deformation behaviour of ti6al4v alloy evaluated by high strain-rate compression tests. *J Mater Process Technol* 75(1–3):127–136
- [14] Lee WS, Chen TH, Huang SC (2010) Impact deformation behaviour of ti-6al-4v alloy in the low-temperature regime. *J Nucl Mater* 402(1):1–7
- [15] Salishchev GA, Zharebtsov SV, Malysheva S, Smyslov A, Saphin E, Izmaylova N (2008) Mechanical properties of ti-6al-4v titanium alloy with submicrocrystalline structure produced by multiaxial forging. *Mater Sci Forum* 584–586:783–788
- [16] Zharebtsov S, Salishchev G, Galeyev R, Maekawa K (2005) Mechanical properties of ti-6al-4v titanium alloy with submicrocrystalline structure produced by severe plastic deformation. *Mater Trans* 46(9):783–788
- [17] Gupta RK, Kumar VA, Mathew C, Rao GS (2016) Strain hardening of titanium alloy ti6al4v sheets with prior heat treatment and cold working. *Mater Sci Eng A* 662:537–550.
- [18] Guo P, Zhao Y, Zeng W, Hong Q (2013) The effect of microstructure on the mechanical properties of tc4-dt titanium alloys. *Mater Eng A Struct Mater Prop Microstruct Process* 563:106–111
- [19] Wahed MA, Gupta AK, Singh SK, Kotkunde N (2018) Effect of anisotropy on mechanical properties of Ti-6Al-4V in superplastic region 346:012023
- [20] Sheikh-Ali A (2007) On flow stress anisotropy in ti-6al-4v alloy sheet during superplastic deformation. *J Mater Sci* 42(10):3621–3626
- [21] Chen W, Boehlert CJ (2011) Texture induced anisotropy in extruded ti-6al-4v-xb alloys. *Mater Charact* 62(3):333–339
- [22] Yang J, Yu H, Wang Z, Zeng X (2017) Effect of crystallographic orientation on mechanical anisotropy of selective laser melted ti-6al-4v alloy. *Mater Charact* 127:137–145
- [23] Li PH, Guo WG, Yuan KB, Su Y, Li YP (2018) Effects of processing defects on the dynamic tensile mechanical behavior of laser-solid-formed ti-6al-4v. *Mater Char*, 140
- [24] Nakai M, Niinomi M, Hieda J, Cho K, Nagasawa Y, Konno T et al (2014) Reduction in anisotropy of mechanical properties of coilable ( $\alpha+\beta$ )-type titanium alloy thin sheet through simple heat treatment for use in next-generation aircraft applications. *Mater Sci Eng A* 594:103–110.
- [25] Wang L, Zhang H, Huang G, Cao M, Cao X, Mostaed E et al (2016) Formability and anisotropy of the mechanical properties in commercially pure titanium after various routes normal and different speed rolling. *J Mater Res* 31(21):3372–3380
- [26] Yu W, Lv Y, Li S, Wang Y, Li B, Liao Z (2015) Mechanism of the anisotropy of yield ratio in ta5 titanium alloy plates. *Mater Sci Eng A* 639:314–319
- [27] Zhu Y, Tian X, Li J, Wang H (2015) The anisotropy of laser melting deposition additive manufacturing ti-6.5al-3.5mo-1.5zr-0.3si titanium alloy. *Mater Des* 67:538–542
- [28] A, H. Z., A, K. Z., A, H. Z., A, Z. L., B, C. Z., & B, X. Y. (2015) Effect of strain rate on microstructure evolution of a nickel-based superalloy during hot deformation—sciencedirect. *Mater Des* 80:51–62
- [29] Balluffi RW, Bristowe PD et al (1981) Structure of high-angle grain boundaries in metals and ceramic oxides. *J Am Ceram Soc*
- [30] Shi W, Yuan L, Xu F, Zheng Z, Shan D (2018) Refining whisker size of 2024al/al 18 b 4 o 33 w composite through extrusion and its effects on the material's micro-structures and mechanical properties. *Mater Charact* 138:98–106

- [31] Dayananda GN, Rao MS (2008) Effect of strain rate on properties of superelastic niti thin wires. *Mater Sci Eng A* 486(1–2):96–103
- [32] Zaiemyekheh Z, Liaghat GH, Ahmadi H, Khan MK, Razmkhah O (2019) Effect of strain rate on deformation behavior of aluminum matrix composites with Al<sub>2</sub>O<sub>3</sub> nanoparticles. *Mater Sci Eng A* 753:276–284
- [33] Barlat F, Glazov MV, Brem JC, Lege DJ (2002) A simple model for dislocation behavior, strain and strain rate hardening evolution in deforming aluminum alloys. *Int J Plast* 18(7):919–939
- [34] Guo WG, Nemat-Nasser S (2006) Flow stress of nitronic-50 stainless steel over a wide range of strain rates and temperatures. *Mech Mater* 38(11):1090–1103
- [35] Wang CJ, Deng KK, Li JC, Liang W (2018) Flow stress and deformation behavior of fine-grained mg matrix influenced by bimodal size sicmp. *J Mater Res* 33(12):1723–1732
- [36] Stricker M, Weygand D (2015) Dislocation multiplication mechanisms—glissile junctions and their role on the plastic deformation at the microscale. *Acta Mater*
- [37] Benzing JT, Poling WA, Pierce DT, Bentley J, Findley KO, Raabe D et al (2018) Effects of strain rate on mechanical properties and deformation behavior of an austenitic fe-25mn-3al-3si twip-trip steel. *Mater Sci Eng A* 711:78–92
- [38] Han Y, Yan S, Yin B, Li H, Ran X (2018) Effects of temperature and strain rate on the dynamic recrystallization of a medium-high-carbon high-silicon bainitic steel during hot deformation. *Vacuum*.
- [39] Hu P, Liu Y, Zhu Y, Ying L (2016) Crystal plasticity extended models based on thermal mechanism and damage functions: application to multiscale modeling of aluminum alloy tensile behavior. *Int J Plast*, pp 1–25
- [40] Manikandan P, Trinadh VV, Bera S, Narasimhan TSL, Joseph M (2016) High temperature mass spectrometric studies on usbnd ga system: thermodynamic properties over (u<sub>3</sub>ga<sub>5</sub>+uga<sub>2</sub>) and (uga<sub>2</sub>+uga<sub>3</sub>) phase regions. *J Nucl Mater* 475:87–93
- [41] Hongmei C, Lei Z, Jianhui B (2016) The effect of grain boundary energy on the amorphous forming composition range of zr–fe–al ternary system. *J Non Crystall Solids*
- [42] Lin YC, Huang J, He DG, Zhang XY, Wu Q, Wang LH, Chen C, Zhou KC (2019) Phase transformation and dynamic recrystallization behaviors in a ti55511 titanium alloy during hot compression. *J Alloys Comp*, 795:471–482
- [43] Griffiths D (2015) Explaining texture weakening and improved formability in magnesium rare earth alloys. *Mater Sci Technol* 31(1):10–24
- [44] Stapleton AM, Raghunathan SL, Bantounas I et al (2008) Evolution of lattice strain in Ti–6Al–4V during tensile loading at room temperature. *Acta Mater* 56(20):6186–6196
- [45] Li H, Boehlert CJ, Bieler TR et al (2015) Examination of the distribution of the tensile deformation systems in tension and tension-creep of Ti-6Al-4V (wt.%) at 296 K and 728 K. *Philosophical Magazine*, 95(7):691–729.
- [46] Bieler TR, Semiatin SL (2002) The origins of heterogeneous deformation during primary hot working of Ti–6Al–4V[J]. *Int J Plast* 18(9):1165–1189
- [47] Zhang J, Di H, Wang H, Mao K, Ma T, Cao Y (2012) Hot deformation behavior of ti-15-3 titanium alloy: a study using processing maps, activation energy map, and zener–holomon parameter map. *J Mater Sci* 47(9):4000–4011
- [48] Ghasemi E, Zarei-Hanzaki A, Farabi E, Tesa K, Ger AJ, Rezaee M. (2016) Flow softening and dynamic recrystallization behavior of bt9 titanium alloy: a study using process map development. *J Alloys Comp*, S0925838816334582.
- [49] Zheng G, Mao X, Li L, Dang R (2018) The variation of microstructures, textures and mechanical properties from edge to center in cross section of ti6242s titanium alloy. *Vacuum*, pp 160
- [50] Wright SI, Nowell MM, Field DP (2011) A review of strain analysis using electron backscatter diffraction. *Microsc Microanal* 17(3):316–329
- [51] Evers LP et al (2004) Scale dependent crystal plasticity framework with dislocation density and grain boundary effects. *Int J Solids Struct* 41(18–19):5209–5230
- [52] Gao H, Huang Y (2003) Geometrically necessary dislocation and size-dependent plasticity. *Scripta Mater* 48(2):113–118
- [53] Calcagnotto M, Ponge D, Demir E et al (2010) Orientation gradients and geometrically necessary dislocations in ultra-fine grained dual-phase steels studied by 2D and 3D EBSD. *Mater Sci Eng A* 527(10–11):2738–2746

**Publisher's Note** Springer Nature remains neutral with regard to jurisdictional claims in published maps and institutional affiliations.